

Review

Characterization of Halogen Bonded Adducts in Solution by Advanced NMR Techniques

Gianluca Ciancaleoni 

Dipartimento di Chimica e Chimica Industriale, Università degli Studi di Pisa, via Giuseppe Moruzzi, 13, 56124 Pisa, Italy; gianluca.ciancaleoni@unipi.it; Tel.: +39-050-221-9233

Received: 7 September 2017; Accepted: 20 September 2017; Published: 25 September 2017

Abstract: In the last 20 years, a huge volume of experimental work into halogen bonding (XB) has been produced. Most of the systems have been characterized by solid state X-ray crystallography, whereas in solution the only routine technique is titration (by using ^1H and ^{19}F nuclear magnetic resonance (NMR), infrared (IR), ultraviolet–visible (UV–Vis) or Raman spectroscopies, depending on the nature of the system), with the aim of characterizing the strength of the XB interaction. Unfortunately, titration techniques have many intrinsic limitations and they should be coupled with other, more sophisticated techniques to provide an accurate and detailed description of the geometry and stoichiometry of the XB adduct in solution. This review will show how crucial information about XB adducts can be obtained by advanced NMR techniques, nuclear Overhauser effect-based spectroscopies (NOESY, ROESY, HOESY . . .) and diffusion NMR techniques (PGSE or DOSY).

Keywords: halogen bonding; supramolecular chemistry; NMR spectroscopy

1. Introduction

The attractive interaction between halogen atoms and nucleophilic species (hereafter called “halogen bond” or “XB”) has drawn the attention of chemists since 1954, when Hassel discovered that the Br–O distance in the 1:1 adduct between Br_2 and dioxane was only 2.71 Å, smaller than the sum of the corresponding van der Waals radii (3.35 Å) [1]. The adduct was immediately recognized as a charge-transfer pair [2], but the details of the interactions were largely unknown. To date, a huge body of experimental and theoretical data [3–7] has been collected, producing a detailed knowledge of the XB interaction and making it a routinely used tool in many fields of chemistry.

In 2013, the International Union of Pure and Applied Chemistry (IUPAC) released a definition for XB, stating that: “A halogen bond occurs when there is evidence of a net attractive interaction between an electrophilic region associated with a halogen atom in a molecular entity and a nucleophilic region in another, or the same, molecular entity” [8]. The easiest way to evidence a net attractive interaction is to measure the interatomic distance, as Hassel did in 1954, between the halogen and the nucleophile in the solid-state. For this reason, X-ray crystallography is the main technique used to characterize halogen-bonded adducts. The large amount of structures produced allows many interesting contributions based on the analysis of structural databases [9–13]. And, indeed, most of the applications of XB are in the materials science: porous systems [14–16], liquid crystals [17], light-emitting materials [18,19] and magnetic materials [20,21] are only some applicative fields fruitfully explored with XB-based materials.

More recently, XB found applications also in solution, mostly for anion recognition [22–24] and catalysis [25–27], with the difference that structural characterization in solution is much more complicated than in the solid state, since most of the experimental techniques are less “direct” than X-ray crystallography. The general method, in the case of an intermolecular interaction, is to monitor a property of the system, which often (but not necessarily) is a spectroscopic observable, in the absence and the presence of that interaction. In most cases, information is derived under the hypothesis that the entire effect on the observable is due to the interaction under examination.

For example, the most used technique for the characterization of XB adducts in solution is titration [28]. It can be performed by using any NMR-active nucleus of the pair (generally ^1H or ^{19}F for their high sensitivity and favorable isotope abundance), even if, depending on the nature of the system, Raman, IR and UV–V is spectroscopies [29,30] can also be used [31]. But the underlying assumption is the same: the effect of the increasing concentration of one component on the chosen property (nuclear magnetic resonance (NMR) chemical shift, infrared (IR) absorption frequency, or whatever) of the second component is supposed to be entirely due to XB. But if two different kinds of adducts were present in solution, one held by XB and the other by a different weak interaction, the disentanglement of the two effects in the experimental data would not be straightforward.

Another critical issue of titration is the stoichiometry of the adduct: each kind of stoichiometry (1:1, 2:1 and so on) requires a different equation for the fitting of titration data, but it can happen that more than one equation satisfactorily fits experimental data, leaving the question to the discretion of the user. A partial solution to the problem is the use of Job's plot, but it is not entirely reliable [28,32].

In both cases, for the structure and the stoichiometry of the adduct, assumptions are generally made on the basis of common sense, or, if the solid-state structure is available, it is just assumed that in solution the adducts have the same structure/stoichiometry. Given the importance of a correct, detailed and accurate characterization of XB adducts, especially when applications in solution are involved, more sophisticated tools should be employed and coupled with classical titrations for a thorough description of the system. Supramolecular chemistry often took advantage of advanced NMR techniques [33–37], especially the nuclear Overhauser effect (NOE)-based NMR spectroscopies [38] and diffusion NMR techniques [39–41]. The former allows the researcher (i) to verify the presence of an adduct (or a particular conformation for intra-molecular interactions) just by detecting a NOE between the nuclei of one fragment with the nuclei of the other; and (ii) to gain information on the relative orientation of the two fragments in the adduct. In a complementary way, the latter allows the direct measurement of the hydrodynamic volume (V_{H}) of the species in solution, thereby revealing if and how much a single species is involved in the formation of supramolecular adducts. Such advanced NMR techniques are, surprisingly, not routinely used in the characterization of XB adducts, but when they are employed crucial information on the behavior of the XB donors and acceptors in solution can be derived, allowing for the correct interpretation of other experimental data (titrations, for example).

In this review, after some examples on the application of 1D NMR techniques, the basic principles of NOE-based spectroscopies and diffusion techniques will be briefly presented. The paper will then show how informative and useful they can be, through a critical discussion of a selection of recently published papers.

2. 1D Nuclear Magnetic Resonance (NMR) Techniques: Applications

Most of the XB systems studied by solution NMR merely take advantage of standard 1D NMR techniques, as the measurement of the chemical shift in different solvents or in the presence of increasing concentration of another component (titration, or Job's plot). Indeed, the information that can be extracted by this reliable, fast and simple technique is impressive.

Already by 1979, Bertrán and Rodríguez had used ^1H NMR spectra to demonstrate the presence of XB in solution [42], using the difference of δ_{CH} in cyclohexane (a very weakly interacting solvent) and in the solvent of interest. Interestingly, very good correlations arose from the results of iodo- and bromoform, whereas the correlations between the results of iodo- and chloroform were poor. This was likely due to the weakness of the chloroform/solvent XB and to the strength of chloroform/solvent hydrogen bonding (HB).

Similarly, Metrangolo and Resnati compared the XB interaction between halogenated hydrocarbons and different solvents by means of ^{19}F NMR spectroscopy [43], measuring for each solvent the value of $\Delta\delta_{\text{-CF}_2\text{X}}$, which is the difference between the chemical shift of the fluorine in the $\text{-CF}_2\text{X}$ moiety in pentane and in the solvent of choice. Results showed that the interaction depends on the nature of X ($\Delta\delta_{\text{-CF}_2\text{I}} > \Delta\delta_{\text{-CF}_2\text{Br}} > \Delta\delta_{\text{-CF}_2\text{Cl}}$) and the solvent; that $\Delta\delta_{\text{-CF}_2\text{I}}$ decreases passing from

primary to tertiary amines; and that, regarding pyridine derivatives, the methyl groups in positions 2 and 6 decreases $\Delta\delta_{\text{-CF}_2\text{I}}$ with respect to the unsubstituted pyridine, likely due to the steric hindrance, whereas electron-donating (withdrawing) groups in position 4 tend to increase (decrease) $\Delta\delta_{\text{-CF}_2\text{I}}$.

Clearly, other nuclei can also provide useful information, especially in those cases in which there are no hydrogen or fluorine nuclei close to the interaction site, or their response is too slight to be accurate. Erdelyi and co-workers demonstrated the applicability of ^{15}N NMR spectroscopy, which is useful for medium/strong XBs [44,45], but is not accurate enough for weak ones (in particular, pyridine and para-substituted halobenzenes) [46]. On the same topic, Philp and co-workers demonstrated that in the case of a iodotriazole having a pending pentafluorophenyl moiety, the ^{19}F δ is almost insensitive to the addition of a pyridine, making titration unsuccessful; whereas monitoring the chemical shift of the nitrogen in the pyridine at increasing concentrations of the iodotriazole (through the ^1H - ^{15}N heteronuclear multiple-bond correlation spectroscopy (HMBC) 2D NMR technique to shorten the acquisition time) led to the determination of the association constant (K_a) [47]. On the other hand, Goroff and co-workers demonstrated the usefulness of ^{13}C NMR spectroscopy and, analyzing the spectra of two iodoalkynes [48], showed that the frequency of the α -carbon is not strictly correlated to the polarity of the solvent, but to the solvent basicity.

The analysis of ^{13}C NMR spectra led also to another interesting result: in a paper by Wang and co-workers, published in 2012, the authors analyzed the trend of ^{13}C NMR δ of $\text{C}_6\text{F}_5\text{X}$ ($\text{X} = \text{Cl}, \text{Br}$) with the concentration in different solvents, concluding that in some cases XB is not the only weak interaction active in solution [49]. Indeed, depending on the nature of X and of the solvent, a competitive lone pair- π interaction is also possible, favored by the electronic depauperation of the aromatic ring due to the presence of the fluorine atoms [50,51].

It is also noteworthy that nuclei different to ^1H are of fundamental importance in solid-state NMR studies on XB [52–54].

For quantitative information, as mentioned in the Introduction, ^1H and ^{19}F NMR titrations are generally very useful. For example, Cabot and Hunter published a systematic study on the values of K_a for many IC_6F_{13} (**II**)-B XB adducts [55], where B is a Lewis base, such as *tri-n*-butylphosphine oxide, an amine or pyridine, in three representative solvents: benzene, CCl_4 and chloroform. Notably, in the latter, $\log K_a$ is positive only when $\text{B} =$ quinuclidine, 1,4-diazabicyclo[2.2.2]octane (**DABCO**) or piperidine, an indication that the XB between neutral species is generally measurable only in apolar solvents. In the case of anionic XB acceptors, K_a can also be large in polar solvents [56,57]. The implicit approximation of all the titrations is that the entire effect is due to XB while, as mentioned, other non-XB adducts can be present. Obviously, this is especially important for weaker XBs, for which the approximation is less acceptable.

Another 1D NMR technique that is used in the characterization of XB in solution is Job's plot. Such a technique is often used in supramolecular chemistry to elucidate the stoichiometry of an adduct, and is based on the concept that the concentration of a D_mA_n complex is at maximum when the $[\text{D}]/[\text{A}]$ ratio is equal to m/n . Unfortunately, this method is reliable under two conditions: (i) D_mA_n is the only adduct present in solution; and (ii) the two components do not self-aggregate [28,32]. Sometimes, if the X-ray structure of the adduct is available, it can be assumed that the stoichiometry in solution is the same, but this assumption is not always safe (see later). Clearly, an accurate determination of the stoichiometry is always desirable, since the equation used to fit the experimental data of a titration depends on the stoichiometry of the adduct. In principle, titration data could be fitted with many equations and the stoichiometry could be decided on the basis of the goodness of the fitting results but, especially for many-body adducts, it is possible that more than one equation satisfactorily fit the data, leaving the final decision to the user. In some cases, it is difficult to find a binding model that fits the experimental data, because of a non-conventional trend in the data, as in the case of sulfate in reference [58].

Many of the potential problems exposed up to now can be solved by combining 1D NMR techniques with advanced NMR ones, as the next sections will elucidate. Anyway, it is important

to underline that the verb “combine” has been used, and not “substitute”, as 1D NMR techniques are rapid, reliable, do not require a special technical training and, in many cases, more advanced techniques merely corroborate the results obtained with 1D methods.

3. Advanced NMR Techniques: Theory

3.1. Nuclear Overhauser Effect

The nuclear Overhauser effect (NOE) arises from the dipole–dipole interaction between NMR-active nuclei, and depends on the competition between multiple- and zero-quantum relaxation mechanisms [59,60]. If we consider two not scalarly-coupled spins, namely I and S , separated by the distance r_{IS} , they have four energy levels, according to the spin states of the two spins ($\alpha\alpha$, $\alpha\beta$, $\beta\alpha$ and $\beta\beta$). The rate constant for the transition between the $\alpha\alpha$ and the $\beta\beta$ states is denoted W_{2IS} (the “2” indicates it is a double-quantum transition), whereas the rate constant for the transition between the $\alpha\beta$ and the $\beta\alpha$ states is denoted W_{0IS} (the “0” indicates it is a zero-quantum transition). The difference between W_{2IS} and W_{0IS} is called the cross-relaxation rate constant and it is generally abbreviated with the symbol σ_{IS} . The basis of NOE is given by the Solomon equation (Equation (1)).

$$\frac{d(I - I^0)}{dt} = -R_I(I - I^0) - \sigma_{IS}(S - S^0) \quad (1)$$

where the apex “0” indicates the equilibrium state; R_I is the self-relaxation rate constant of the spin I (the sum of all the possible rate constants W); and the transition between I (or S) and $2IS$ are neglected (formally, $\Delta_I = \Delta_S = 0$). Equation (1) says that when S spin magnetization deviates from the equilibrium, the I spin magnetization will change proportionally to σ_{IS} and to the extent of the deviation of the S spin from the equilibrium. Clearly, the cross-relaxation term must be different to zero and, since the two spins are not scalarly coupled, this happens only when there is a dipolar relaxation between I and S . In the steady state NOE, and for a system isotropically tumbling in solution, Equation (1) can be written as in Equations (2)–(4).

$$NOE_I\{S\} = \frac{I - I^0}{I^0} = \frac{\gamma_S \sigma_{IS}}{\gamma_I \rho_{IS}} \quad (2)$$

$$\sigma_{IS} = \left(\frac{\mu_0}{4\pi}\right)^2 \frac{\hbar^2 \gamma_I^2 \gamma_S^2}{10} \left(\frac{6\tau_c}{1 + (\omega_I + \omega_S)^2 \tau_c^2} - \frac{\tau_c}{1 + (\omega_I - \omega_S)^2 \tau_c^2} \right) r_{IS}^{-6} \quad (3)$$

$$\begin{aligned} \rho_{IS} &= W_{2IS} + 2W_{1I} + W_{0IS} \\ &= \left(\frac{\mu_0}{4\pi}\right)^2 \frac{\hbar^2 \gamma_I^2 \gamma_S^2}{10} \left(\frac{6\tau_c}{1 + (\omega_I + \omega_S)^2 \tau_c^2} + \frac{3\tau_c}{1 + \omega_I^2 \tau_c^2} \right. \\ &\quad \left. - \frac{\tau_c}{1 + (\omega_I - \omega_S)^2 \tau_c^2} \right) r_{IS}^{-6} \end{aligned} \quad (4)$$

where μ_0 is the permeability constant in a vacuum; \hbar is the Planck’s constant divided by 2π ; τ_c is the rotational correlation time; ω_I and ω_S are the resonance frequencies of I and S nuclei, respectively; and ρ_{IS} is the dipolar longitudinal relaxation rate constant. The dependence of both σ_{IS} and ρ_{IS} on r^{-6} implies that the steady-state NOE cannot be directly related to the internuclear distances. For an estimation of the latter, the measurement of the kinetics of the NOE buildup, i.e., the measurement of NOE at different values of mixing time (τ_m), is needed (Equation (5))

$$NOE_I\{S\}(\tau_m) = e^{-(R - \sigma_{IS})\tau_m} (1 - e^{-2\sigma_{IS}\tau_m}) \quad (5)$$

where R represents the total longitudinal relaxation rate constants of both I and S spins, assumed to be equal. If quantitative information on r_{IS} is needed, the experimental data should be collected in an

extensive range of τ_m and fitted using Equation (5) (Figure 1); or, if only small values of τ_m are used (linear buildup), the data can be fitted with a straight line, whose slope will be equal to $2\sigma_{IS}$.

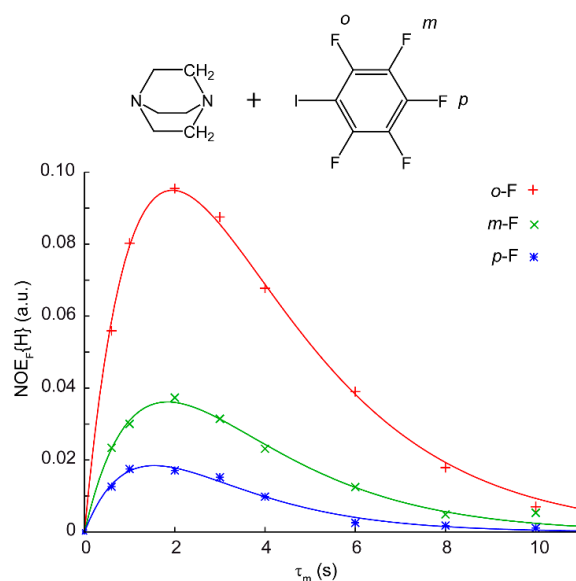


Figure 1. Adapted with permission from reference [61]. Experimental data relative to the intensity of nuclear Overhauser effect (NOE) on the fluorine nuclei of iodopentafluorobenzene as a function of τ_m after the irradiation of CH_2 protons of DABCO. The straight lines are the best fitting functions using Equation (5). Copyright 2015 Wiley-VCH Verlag GmbH & Co. KGaA.

Now, r_{IS} can be evaluated after an evaluation of τ_c , the other variable present in Equation (3), or by comparing σ_{IS} with σ_{AB} , where A and B are a couple of spins of the same nature, whose distance is known and with the same rotational correlation time [62,63]. Under these circumstances, Equation (6) allows the measurement of r_{IS} .

$$\frac{\sigma_{IS}}{\sigma_{AB}} = \left(\frac{r_{IS}}{r_{AB}} \right)^{-6} \quad (6)$$

The simplest pulse sequence to perform 2D NOESY is shown in Figure 2. The first 90° rf pulse rotates the magnetization of the spin I on the xy plane, where it can evolve according to its frequency ω_I and the second 90° rf pulse turns a part of the magnetization back on the z -axis. The size of this magnetization depends on ω_I and t_1 and, therefore, it is said to be a frequency-labelled magnetization. During the mixing time (τ_m), this magnetization can be partly transferred to the spin S by NOE or chemical exchange, keeping its dependence from ω_I in the process. The last 90° rf pulse rotates this z -magnetization back onto the y -axis, where it can be read. The part of the magnetization that did not undergo NOE or exchange will evolve again according to its ω_I , giving a signal at $[\omega_I, \omega_I]$ (diagonal peak), whereas the part that underwent NOE or exchange to spin S will evolve according to ω_S , giving a signal at $[\omega_I, \omega_S]$ (off diagonal peak). Such a simple pulse sequence is not used anymore and many other, more complex sequences have been developed.

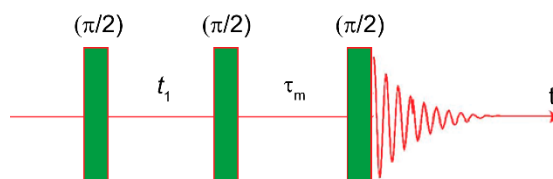


Figure 2. Pulse sequence for the NOE experiment (basic version).

The NOE-based techniques (NOESY, its heteronuclear version HOESY or the experiment performed under spin-locked conditions, ROESY) are therefore of primary importance in the structural elucidation of an adduct, either qualitatively, since the simple detection of a NOE between the nuclei of two molecular entities is already enough to demonstrate the presence of an intermolecular adducts in solution [64], or quantitatively, since the quantification of different NOEs can give precious information on the internal structure and the geometry of the adduct [65,66]. In Section 4, we will see some examples of how NOE spectroscopies can be practically applied in this sense.

Obviously, the potential of the NOE technique goes far beyond the examples here reported, and its possibilities and limitations can also be effectively explored by coupling experimental data with model theories [66–68].

3.2. Diffusion NMR

Comparing the intensity of a NMR signal in the absence and presence of a gradient of the magnetic field along the z axis $G(z)$, the former is always more intense than the latter. What is responsible for this attenuation is the translational self-diffusion [69,70], that is, the net result of the thermal motion induced by the random Brownian motion experienced by particles or molecules in solution. Starting from this, it can be understood that by performing a series of spectra at different values of G , the translational self-diffusion coefficient (D_t) can be directly measured plotting the signal attenuation as a function of G .

In more detail, the basis of diffusion NMR techniques rely on the fact that the Larmor frequency (ω) depends on the strength of the magnetic field and on the gyromagnetic ratio (γ) of the nucleus of choice. In the presence of a homogenous magnetic field B_0 , ω has the same value at every position of the sample (Equation (7)).

$$\omega = \gamma B_0 \quad (7)$$

If a second magnetic field, whose intensity linearly depends on z ($G(z)$, [$T\ m^{-1}$]) is added to B_0 , homogeneity is lost and Equation (7) can be written as a function of the z coordinate (Equation (8)).

$$\omega = \gamma(B_0 + G(z) \cdot z) \quad (8)$$

Now, ω depends on the position of the nucleus, but how this labeling can be used to measure D_t requires a short discussion of the actual pulse sequence.

The simplest pulse sequence is a modification of the spin-echo sequence published by Hahn in 1950 [71], proposed by Stejskal and Tanner in 1965 (Figure 3) [72].

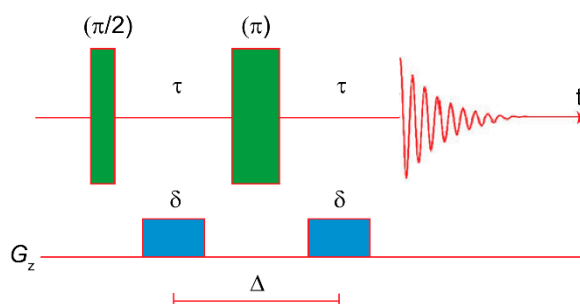


Figure 3. Pulse sequence for the pulsed-field gradient spin echo (PGSE) experiment (basic version).

The first act is a 90° rf pulse that rotates the magnetization on the xy plane, where it undergoes many dephasing phenomena: chemical shift, hetero- and homonuclear J -coupling evolution, and spin-spin transverse relaxation (T_2). Furthermore, the presence of a gradient introduces an additional dephasing component. At $t = \tau$, a 180° rf pulse is applied. This inverts the precession direction and the dephasing turns into a rephasing phenomenon. During this time, another gradient is applied, exactly equal to the first one, with the aim of recreating the conditions of the first τ

period and, consequently, generating an echo at $t = 2\tau$. The net result is the conventional spectrum, distorted for the J -coupling and weighted for the T_2 . But the nuclei that in the first τ period were in the position z' , were in the second τ period in the position z'' because of the Brownian motion. Consequently, they experience two different magnetic fields during the dephasing and the rephasing periods, which causes an incomplete rephasing and, therefore, an attenuation of the signal intensities. Such attenuation depends on the difference between z' and z'' and, since small molecules diffuse faster than large ones, the attenuation for the former will be more severe than for the latter, leading to a discrimination of the species in solution depending on their D_t (Figure 4).

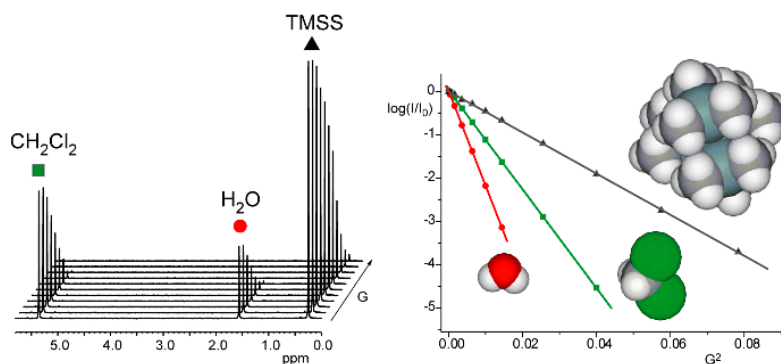


Figure 4. Reproduced from ref. [73]. Left: A series of 1D nuclear magnetic resonance (NMR) spectra recorded at different G values. Right: Plot of the $\log(I/I_0)$, where I and I_0 are the intensities of the signals in the presence and in the absence of G , respectively, vs. G^2 . Note the inverse proportionality between the slope of the fitting line and the molecular size.

Equation (9) describes the relationship between the intensity of a signal (I) and D_t .

$$I(2\tau) = I(2\tau)_{G=0} \cdot e^{(-\gamma^2 G^2 \delta^2 D_t (\Delta - \frac{\delta}{3}))} \quad (9)$$

where I and I_0 are the intensities of a signal at time 2τ in the presence and in the absence of G [74]. By performing a series of spectra with different values of G , the experimental data can be fitted and D_t can be evaluated. This technique is generally called pulsed-field gradient spin echo (PGSE). Also, in this case many other more complex pulse sequences are available. Processing the data as a 2D spectrum with chemical shifts on the F2 axis and diffusion constants on the F1 axis, a diffusion-ordered NMR spectroscopy (DOSY) plot is obtained.

The subsequent passage from D_t to the hydrodynamic volume is possible through the Stokes–Einstein equation [75] successively modified by Chen for medium-size molecules [76]. The experimental conditions and data-processing are particularly important to obtain accurate values of D_t , and useful instructions can be found in reference [73], which illustrates, among other things, the importance of the internal standard and what to do in the presence of non-spherical species.

Taking advantage of this, diffusion NMR techniques, can be used in different ways: for example, if the NMR sample is contaminated with one or more solvents whose signals overlap with the compound of interest, the application of a small gradient will eliminate, partially at least, such signals [77]. More quantitative information can be useful in determining the molecular weight distribution for polymers [78], the purity and composition of functionalized carbon nanotubes [79], the formation of ion pairs and quadruples [80–83], or, in the case of neutral species, of supramolecular adducts [84,85].

4. Advanced NMR Techniques: Applications

4.1. Nuclear Overhauser Effect

The first paper employing a NOE analysis for the structural characterization of a XB system in solution, to the best of my knowledge, was published in 2004 by Tatko and Waters [86]. In this paper, the authors synthesized a model β -hairpin peptide and demonstrated that, in water, the substitution of a hydrogen with a halogen has a stabilizing effect on the folded conformation ($\Delta\Delta G = -0.12, -0.34, -0.47$ and -0.54 for F, Cl, Br and I, respectively; $\Delta\Delta G = -1.01$ kcal/mol in the case of substitution of two hydrogens with iodine atoms). The NOE analysis was important to ensure that (i) the conformation was folded; and (ii) the iodine was actually facing the aromatic ring of the N-terminal phenylalanine, allowing the authors to demonstrate the presence of the halogen- π interaction. They also studied the impact of the substitution on the thermodynamic parameters of the folding, finding out that the presence of iodine provides an enthalpic driving force but also an additional entropic cost. Combining these results with other thermodynamic data, the authors concluded that dispersion forces are responsible for the improved stability.

In 2010, Beer and coworkers synthesized some interlocked host systems in which a chloride is held into the macrocycle **1** (Figure 5) by two HBs and, at the same time, a functionalized imidazolium **2a-e** interacts with the chloride by XB or HB [87].

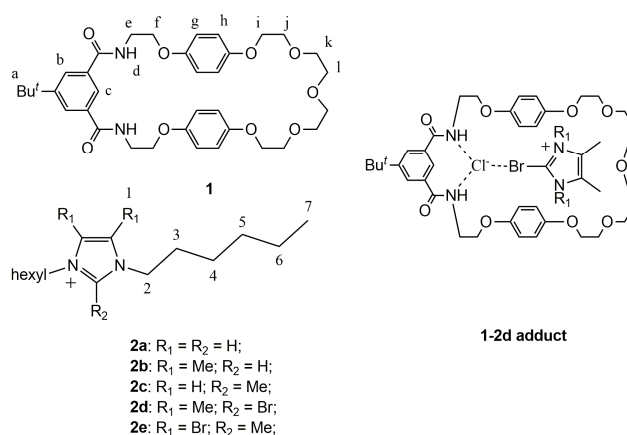


Figure 5. Numbering of the compounds studied in reference [87] and structure of the **1-2d** adduct.

The whole system is held together by a mixture of weak interactions (ion pairing, HB, π - π stacking, XB), but the orientation of the imidazolium moiety and the strength of the K_a is dictated by the functional groups. In the case of **1-2a** or **1-2b**, the hydrogen in the 2-position of the imidazolium interacts with the chloride, in both cases with a K_a around $95 M^{-1}$. In the case of **1-2c**, the 2-position is occupied by a methyl group and the HB is not possible any more. Despite this, K_a is much higher than before ($245 M^{-1}$). Analyzing the pattern of chemical shifts, the authors conclude that for **1-2c**, the orientation of **2c** is different than before and now the hydrogens in position 4 and 5 interact with the chloride; while the methyl in position 2 establishes an additional weak HB with the oxygens, explaining the increased value of K_a . The authors employed 1H ROESY for the characterization of **1-2d**, demonstrating not only that the adduct was formed, but also that the bromine in position 2 is facing the chloride (Figure 6). Indeed, the two methyl moieties in position 4 and 5 of **2d** (number 1 in Figure 6) show NOE intermolecular contacts with the protons g/h/k/l/j, which are far from the amine moieties, whereas there are no NOE contacts with the protons e/f/d, which are close to the amine moieties.

Notably, $K_a(\mathbf{1-2d}) = 254 \text{ M}^{-1}$, demonstrating that in some cases XB can be more efficient than HB in the construction of supramolecular adducts. The insertion of bromine in positions 4 and 5 or the substitution of Cl^- with PF_6^- did not lead to the formation of the adduct.

The same research group recently used systems similar to **1** to create catenane systems [88], also in this case using multiple weak interactions together to form a supramolecular adduct and, in a second step, closing the second cycle through a Grubbs-catalyzed ring closing metathesis. The final catenane system selectively binds iodide and bromide anions, whereas there is no evidence of binding in the presence of acetate anions.

Inspired by the Wang's paper [49], Ciancaleoni and others recently used the ^{19}F , ^1H HOESY technique to study in detail the structure in solution of small and well-known XB adducts and find other evidences of the contemporary presence of XB and non-XB adducts [61]. Given the excellent electron-withdrawing properties of fluorine, this nucleus is present in many XB systems, making ^{19}F , ^1H HOESY a technique with a great potential. In fact, given the high directionality of XB [89,90], the geometry of a XB adduct and, therefore, the NOE intermolecular pattern, can be accurately predicted. For this, any deviation of the experimental pattern from the predicted one can be due to the presence of other weak interactions, and, consequently, of adducts with a different geometry than that of the XB one.

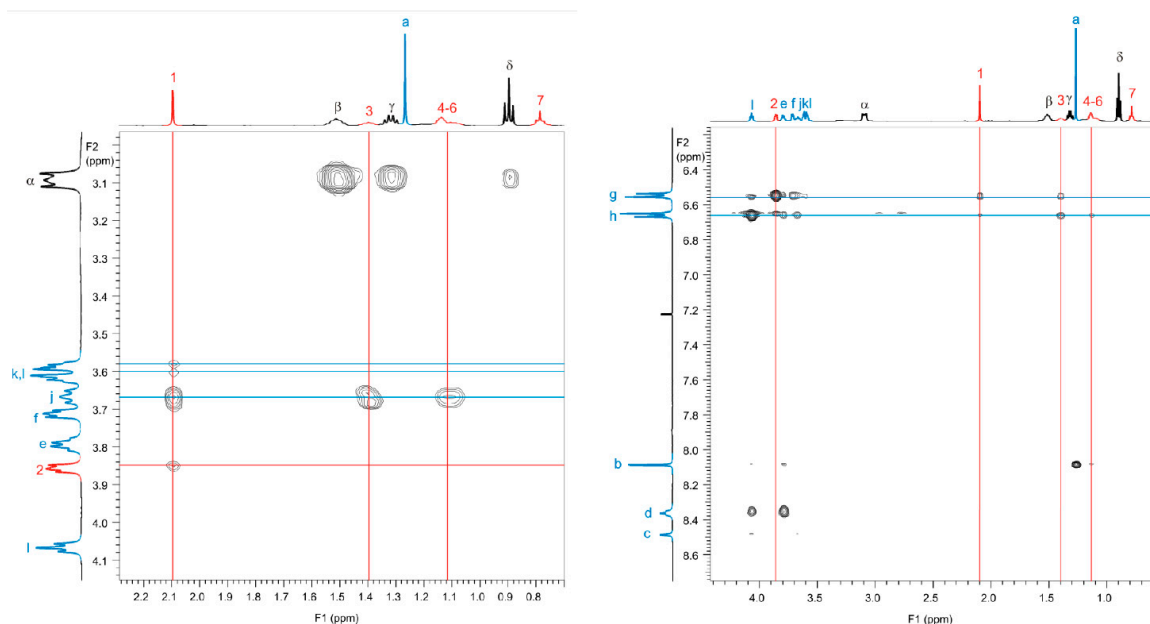


Figure 6. Reproduced from reference [87]. Through-space coupling between protons on imidazolium chloride **2d** and the posterior polyether protons of **1** (left) and between protons on imidazolium chloride **2d** and the hydroquinone protons of **1** (right). Blue and red peaks refer to compound **1** and **2d**, respectively. Labels in greek refer to the tetrabutylammonium cation. Copyright 2010 Wiley-VCH Verlag GmbH & Co. KGaA.

For example, considering **DABCO** and perfluorohexyl iodide (**I1**), the $\alpha\text{-F}/\text{-CH}_2\text{-}$ (whereas α refers to the fluorine atoms germinal to the iodine) heteronuclear NOE contact is a good indicator for the presence of the XB adduct. Experimentally, the $\alpha\text{-F}/\text{-CH}_2\text{-}$ contact is clearly visible (solvent = benzene- d_6), but also the $\gamma\text{-F}/\text{-CH}_2\text{-}$ contact is strong, even stronger than the $\alpha\text{-F}/\text{-CH}_2\text{-}$ one, whereas the $\beta\text{-F}/\text{-CH}_2\text{-}$ is very weak and all the others are almost undetectable. The reason why the $\gamma\text{-F}/\text{-CH}_2\text{-}$ contact is stronger than the $\alpha\text{-F}/\text{-CH}_2\text{-}$ one can be rationalized by using density functional theory (DFT) calculations: the structure in which the chain is folded is almost isoenergetic to that with the unfolded chain ($\Delta E = 0.6 \text{ kcal/mol}$ at B3LYP-D3/TZVP level of theory). Because of the folding, the $\gamma\text{-F}$ results to be closer to $\text{-CH}_2\text{-}$ than $\alpha\text{-F}$ (4.3 and 5.4 Å, respectively, according to DFT-optimized

geometries). Therefore, the two conformers of the XB adduct can explain all the experimental NOE contacts. On the other hand, other non-XB adducts can be modeled by DFT, but they are higher in energy ($\Delta E = 5.6$ kcal/mol) and can likely be neglected.

The same technique was also applied to the pair **DABCO**/pentafluoriodobenzene (**I2**): given the structure of the XB adduct, only the *ortho*-F/-CH₂- NOE contact should be visible, because it is the only one for which the predicted internuclear distance is reasonable for NOE (5.1, 7.8 and 9.3 Å for *ortho*-, *meta*- and *para*-CH₂ distances, respectively). But experimentally, *meta*-F and *para*-F also give measurable contacts (Figures 1 and 7), the presence of which demonstrates that a portion of the adducts has a different structure and, therefore, is held by other interactions than XB. DFT calculations showed that the lone pair/ π adduct is less stable than the XB one ($\Delta E = 3.0$ kcal/mol at B3LYP-D3/TZVP level of theory), but the internuclear H/F distances are extremely short: 3.3–3.5 Å. Indeed, we need to remember that the intensity of an intermolecular contact depends, among other things, on two parameters: the average H/F distance in that adduct and the concentration of the structure in solution. The former can be derived by theoretical geometry optimizations, which are quite accurate [91], whereas the latter can be approximately evaluated by combining the intensity of NOE contacts, or better, their σ_{HF} constant evaluated by the NOE build-up (Figure 1), and the DFT-derived internuclear distances. According to this strategy, in the **DABCO**/**I2** mixture (solvent = benzene-d₆) 4% of the adducts are held by lone pair/ π interactions and the remaining 96% by XB.

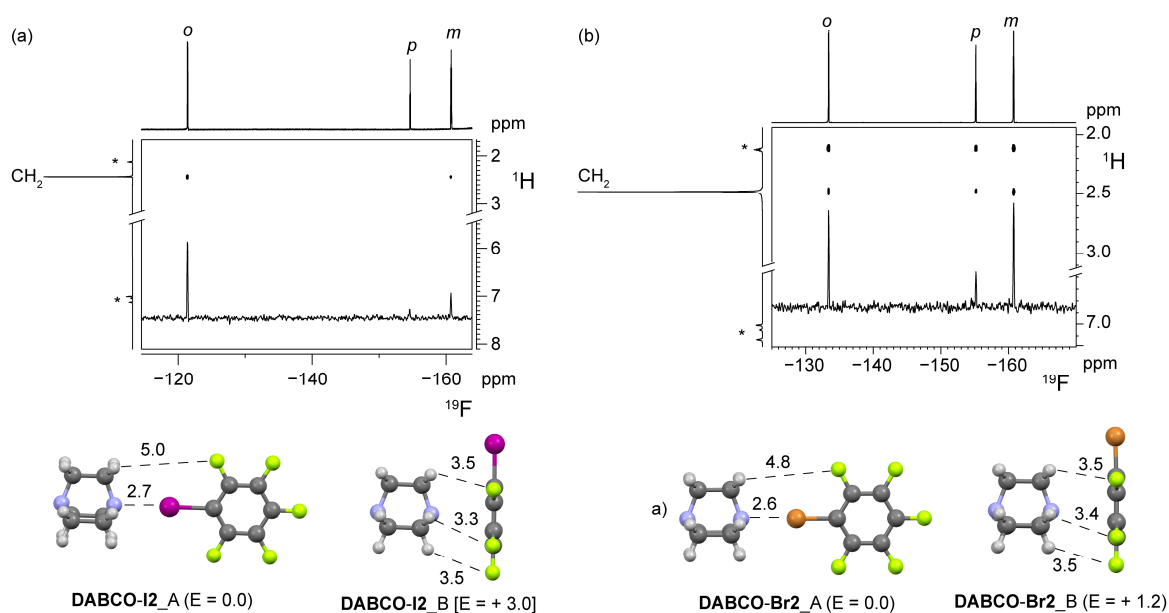


Figure 7. Adapted with permission from reference [61]. ¹⁹F, ¹H HOESY NMR spectrum of a mixture of (a) **DABCO** and **I2** and (b) **DABCO** and **Br2**. The trace is relative to the frequency of the -CH₂-. Asterisks denote residual solvent peaks. Bottom: DFT-optimized geometries for **DABCO**/**I2** and **DABCO**/**Br2** adducts with relevant distances and relative energies [kcal mol⁻¹, B3LYP-D3/TZVP level of theory]. Copyright 2015 Wiley-VCH Verlag GmbH & Co. KGaA.

By using pentafluorobromobenzene (**Br2**), the *meta*-F/-CH₂- NOE contact is as intense as the *ortho*-F/-CH₂- one (Figure 7). The relative concentration of XB and non-XB adducts can be evaluated as 56:44. In this case, it is clear that a titration is not enough to accurately establish the strength of the XB, since the contribution of the two structures to the physical property (a NMR chemical shift, a UV-Vis absorbance peak . . .) should firstly be disentangled before the fitting [92].

In 2017, Jiang and co-workers synthesized a series of alanine-based halogen-substituted bilateral N-amidothiureas containing two β -turns structural motifs. An X-ray of the crystal structure demonstrated that the monomer self-organizes in supramolecular helices held together by iodine . . .

π interactions, while other inter-helices XBs create a complex network [93]. Substituting iodine with chloride, helical structures do not form in the solid state. Comparing X-ray structures with NOESY spectra, the authors deduced that when $X = \text{Cl}$ (LL-ACl), only intramolecular NOE contacts are visible and, in particular, the e–f contact is clearly visible (internuclear e–f distance in the solid-state structure: 3.189 Å) and the e–g is not (internuclear e–g distance in the solid-state structure: 4.348 Å, Figure 8).

On the contrary, when $X = \text{I}$ (LL-AI), also the e–g contact is visible and, therefore, it should be due to an intermolecular contact rather than intramolecular (inter- and intramolecular internuclear e–g distances in the solid-state structure: 2.368 and 4.550 Å, respectively, Figure 8). The authors underline but do not comment upon the absence of the e–f contact for which both inter- and intramolecular internuclear e–g distances in the solid-state structure (3.686 and 3.106 Å, respectively) should be short enough for a NOE contact. The existence of supramolecular helices is also supported by the peak intensities of LL-AI, which are lower, at the same concentration, than those of LL-ACl. This has been explained by the fact that the formation of the supramolecular helix leads to peak broadening and, therefore, invisibility in the NMR spectrum [94].

Extending the same topic, a double helix held by XBs has also been characterized in the solid state [95], whereas Berryman and co-workers succeeded in synthesizing a triple helix stabilized by XB. For the latter, a complete characterization in solution is also available, including the presence of inter-strand NOE contacts, to verify the helicity and measure the diffusional coefficient in order to further characterize the adduct.

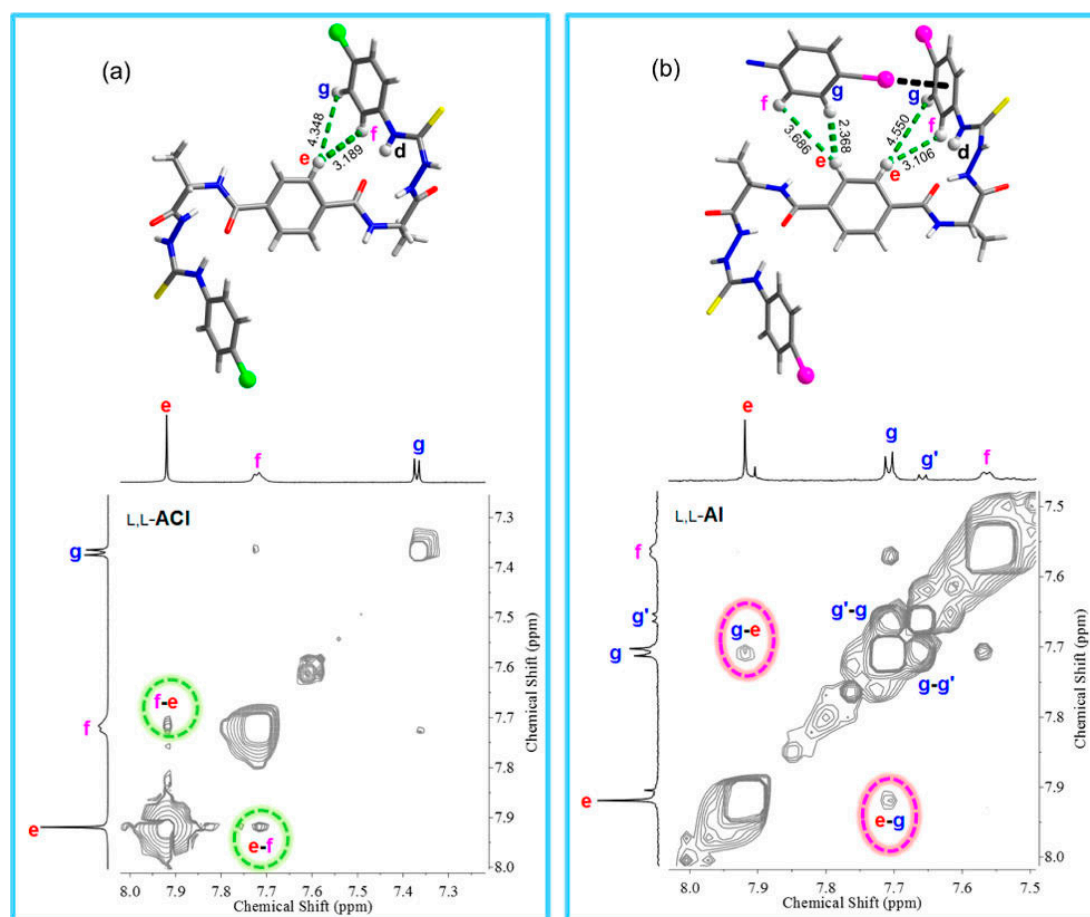


Figure 8. Reproduced from ref. [93]. Sections of ^1H -NOESY spectra showing couplings between protons in phenyl rings in LL-ACl (a) and LL-AI (b). On top, crystal structures are also shown. Copyright 2017 American Chemical Society.

In a very recent work by Erdélyi and co-workers, the authors took advantage of XB to stabilize the β -hairpin conformation in an artificial peptide model system [96]. After optimization of the amino acid sequence and the synthesis of the actual system, all the signals of the NMR spectrum were assigned by a total correlation spectroscopy (TOCSY) NOESY strategy, while the presence of two β -turns were confirmed by the measurement of the $\Delta\delta_{\text{NH}}/\Delta T$ coefficients. Structural information was obtained by measuring the NOE buildup for all the correlations, in order to ascertain the average distance ratios, and the $^3J_{\text{C}\alpha\text{H},\text{NH}}$ values, which were converted in average dihedral angles through a version of the Karplus equation. The experimental data were coupled with restraint-free Monte Carlo calculations, and all the collected data were used as input for the NAMFIS analysis. The latter consists of the generation of a “complete” set of conformation that can potentially contribute to the experimental ensemble by theoretical methods and, in turn, the evaluation of their relative population by comparing experimental and computational data. As a result, the probability of the β -hairpin conformation existing in solution was 74%. Substituting the chlorine atom with a methyl group, the probability for the corresponding HB-stabilized conformer was only 29%. The substitution of chlorine with bromine did not increase the probability of the β -hairpin conformation, as expected, likely because of the higher steric demand of the bromine, which would cause a deformation of the backbone.

These examples demonstrated how NOE-based techniques can be of fundamental importance for the structural identification of simple and complex, inter- and intramolecular XB interactions.

4.2. Diffusion NMR

For diffusion NMR techniques (DOSY or PGSE), the first application, to the best of my knowledge, was in a study published in 2012 by Erdélyi and co-workers, dealing with the characterization of the $[\text{N-X-N}]^+$ bond [97]. The authors started from the fact that the analogous $[\text{N-H-N}]^+$ is generally asymmetric in solution (the central hydrogen is located closer to one basic center, $[\text{N-H} \dots \text{N}]^+$) but symmetric in crystals (the hydrogen is located exactly in the midway between the two basic centers), [98] and synthesized molecular systems in which the N–X distances were free to adjust and others in which they were not. By means of the isotopic perturbation of equilibrium technique through the ^{13}C NMR detection, the authors suggested that, in contrast with HB, XB always prefers to be symmetrical in solution. In addition, the measurement of the diffusion coefficient of the cation (D_i^+) and the anion (D_i^-) allowed them to ascertain that all the systems form tight ion pairs [99] in CD_2Cl_2 . However, even the proximity of the triflate is not enough to perturb the symmetry of the two XBs. It must be said that the simple presence of tight ion pairs could be not enough to perturb a similar system, since the anion should also be located close to the X^+ moiety to exert its effect, which is not obvious [100–103]. In the author’s opinion, since some of the employed anions contains fluorine nuclei, a ^{19}F , ^1H HOESY experiment between the anion and the cation (see above) could have further clarified this point. The $[\text{N-X-N}]^+$ system remains symmetrical, also varying the nature of the anion [104]. A notable exception has been found when $\text{X} = \text{F}$, for which the asymmetric conformation is preferred [105]. Interestingly, in this case the authors did not observe any NOE contact between the fluorine and the pyridine moieties.

In 2012, Beer and co-workers synthesized a macrocyclic halo-imidazolium receptor able to recognize iodide and bromide in water and produce a fluorescence signal as a response [106]. Interestingly, the crystal structure critically depends on the anions: in the presence of two PF_6^- , no XB can be observed between the iodine of the cation and the anion; on the contrary, in the presence of one PF_6^- and an iodide, or bromide, a dimeric structure is found in the solid-state, with two cations interacting with two different halide in a pincer-like arrangement (Figure 9).

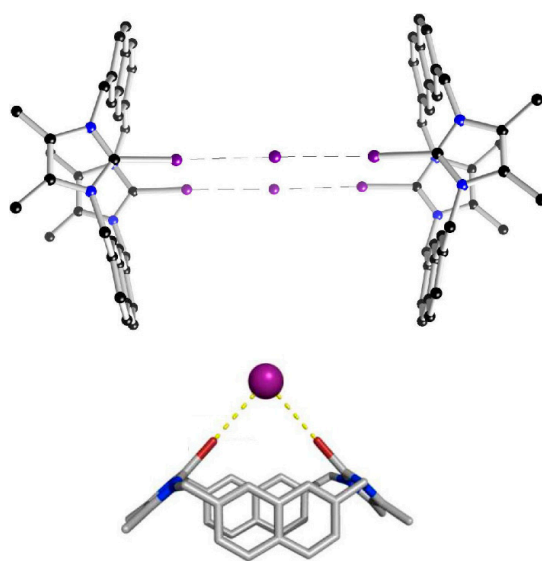


Figure 9. Adapted with permission from reference [106]. (Top) Dimeric crystal structure of iodo-imidazolium (PF_6^- and hydrogens are omitted for clarity) and (bottom) density functional theory (DFT) structure of the monomeric structure present in solution. Copyright 2012 American Chemical Society.

The titration technique produced a very high value of K_a ($>104 \text{ M}^{-1}$) and the Job plot suggested a cation:anion = 1:1 stoichiometry. But the latter cannot exclude the 2:2 structure found in the solid-state, therefore a technique able to determine the absolute hydrodynamic volume of the adduct in solution, as DOSY, was necessary. The authors measured the D_t of the cation with 0, 6 and 10 equivalents of NBu_4I . The presence of a dimeric structure would have led to a decrease of D_t as $[\text{I}^-]$ increased, but the three values of D_t resulted in being very similar, once corrected for the viscosity of the solution. Consequently, only monomers were present in solution. DFT calculations provided a plausible, alternative structure (Figure 9), in which the two iodine atoms form two XBs with the same iodide anion. This structure has also a lower entropic cost. The message of this example is clear and of primary importance: never accept a priori the solid-state structure as a good model for the solution structure. Often they will be similar, but looking for experimental proofs confirming this is always a good idea.

Philp and co-workers synthesized an iodotriazole with a pending pentafluorophenyl moiety, demonstrating that it is a XB acceptor as good as the prototypical **I2** [47]. As already noted, the K_a between the iodotriazole and 4-methylpyridine cannot be estimated through a ^{19}F NMR titration, as the fluorine atoms are too far from the XB acceptor group, but the use of ^1H , ^{15}N HMBC NMR spectroscopy led to a value of 1.67 M^{-1} ($K_a = 2.67 \text{ M}^{-1}$ for the **I2**/4-methylpyridine). The substitution of the *para*-F with a 3-hydroxyl-pyridine group led to a molecule having both XB acceptor and donor groups on the same side, leading, according to DFT calculations, to a stable doubly-halogen bonded homodimer. Interestingly, the solid state structural characterization showed that homodimers were not present and the iodine and the pyridine were connected by XB to different molecules, with the formation of supramolecular chains. In solution, the analysis of the ^1H NMR spectrum at different concentrations led to a self-aggregation constant of 3.4 M^{-1} , indicating that the two XBs behave almost independently from each other. Measuring the D_t of the molecule at different concentrations, the data could be satisfactorily fitted with a dimerization model and the value of D_t remained practically constant between 150 and 200 mM, an indication that a *plateau* had been reached. Combining the value of the self-aggregation constant, which is double with respect to the iodotriazole/4-methylpyridine case, and the trend of D_t vs. the concentration, the homodimer model indeed seems to be more accurate.

Finally, Ciancaleoni and co-workers published a paper completely focused on the NMR diffusion technique as a tool for characterizing single and multi-site XB adducts [107]. Firstly, they show how

converting the values of D_i in volumes, using the corrected version of the Stokes–Einstein equation [73], can make the technique more useful and intuitive. The main advantage is that we can easily predict the volume of the adducts (Equation (10)), since generally the latter is the simple sum of the volumes of its components (this is not true when we deal with D_i or hydrodynamic radius values) [108].

$$V_H^{agg}(\mathbf{nD}, \mathbf{mA}) = n * V_H^0(\mathbf{D}) + m * V_H^0(\mathbf{A})E \quad (10)$$

where n and m are the stoichiometric coefficient in the case of $n:m$ adducts.

The first consequence is that a rough estimation of the K_a can be obtained from a single measurement, as done for the weak interaction between 2,4,6-trimethylpyridine and **I1** (1.6 M^{-1}) by using Equation (11) [109].

$$V_H^{exp}(\mathbf{D}) = \alpha V_H^{agg}(\mathbf{nD}, \mathbf{mA}) + (1 - \alpha) V_H^0(\mathbf{D}) \quad (11)$$

where α is the association coefficient, from which the calculation of K_a is possible. This can be useful, for example, when the low solubility of the adduct or the single component does not allow for a standard titration. But importantly, the value of $1.6 \pm 0.5 \text{ M}^{-1}$ cannot be assigned exclusively to XB, since as ^{19}F , ^1H HOESY data demonstrated [61], in solution the adducts held from a XB between the nitrogen and the iodine coexist with others held from dispersion forces between the fluorinated chain and the hydrogens of the pyridine. As diffusion NMR results depend only on the total presence of the adducts and not on the kind of interaction that lead to the formation of the adduct, 1.6 M^{-1} has to be the sum of all the possible equilibrium constants leading to 1:1 adducts. Interestingly, the K_a measured by the ^{19}F NMR titration is much lower, $0.85 \pm 0.01 \text{ M}^{-1}$. Under the hypothesis that ^{19}F NMR titration results refer exclusively to XB adducts, which is questionable but a likely first approximation, the K_a for non-XB adducts can be estimated as 0.75 M^{-1} .

In the same paper, it is also shown that mixing hexamethylenetetramine (**HMTA**), a base with four equivalent XB-acceptor groups, and N-bromosuccinimide (**NBS**), 1:3 and 1:4 adducts are not present in solution. Also in this case, the use of hydrodynamic volumes made the analysis much easier: since the hydrodynamic volumes of isolated **HMTA** and **NBS** can be easily measured (137 and 189 \AA^3 , respectively), the V_H values of the different adducts can be calculated, and result in being 323 , 457 , 591 and 729 \AA^3 for 1:1, 1:2, 1:3 and 1:4 adducts, respectively. Experimental values for $V_H(\text{HMTA})$ go from 189 to 438 \AA^3 (in the presence of 0 and 44 equivalents, respectively) confirming the presence of just 1:1 and 1:2 adducts. Actually, 438 \AA^3 is an average value and does not exclude a priori the presence of larger adducts, but analyzing the trend of the data with the concentration it can be seen that $V_H(\text{HMTA})$ reaches a *plateau* in correspondence with the 1:2 adduct (Figure 10), indicating that larger aggregates are absent. Having the stoichiometry of the adduct as an experimental result and not as a hypothesis, the experimental data could be fitted without ambiguity with the correct model. The authors used the theoretical charge displacement function analysis method [110–113] to demonstrate the anti-cooperative nature of XB interactions in this system: when one nitrogen donates electronic density to a **NBS** moiety, the other nitrogens become less basic and, therefore, less able to establish a new XB.

It is also interesting to see that, indeed, in the solid-state structure of **HMTA/NBS** only 1:2 adducts can be detected, whereas substituting **NBS** with *N*-iodosuccinimide (**NIS**), 1:4 adducts are clearly visible [114]. Unfortunately, the **HMTA/NIS** adduct was too insoluble to allow any PGSE measurement.

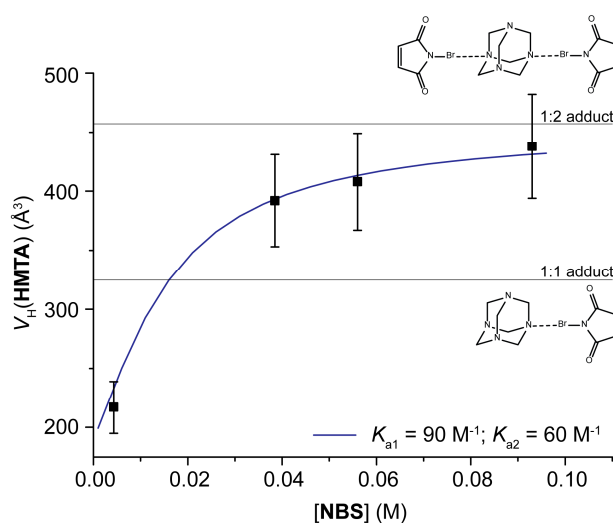


Figure 10. Adapted with permission from reference [107]. Experimental hydrodynamic volume of HMTA ($C = 2.1$ mM) at different concentrations of NBS. The solid line represents the best fitting equation for the 1:2 model. Copyright 2016 The Royal Society of Chemistry.

5. Conclusions

The present review demonstrates that XB adducts in solution should not be characterized only by titration and Job's plot techniques, and the latter should always be coupled with other, more sophisticated techniques enabled by modern NMR spectrometers. The most important information that can be derived concerns the internal structure (NOE) and the size (diffusion) of the adduct; but, depending on the system studied, the presence of competing interactions beyond the XB and the value(s) of equilibrium constants and thermodynamic parameters can also be derived. In some cases, the combination of experimental data with theoretical results is beneficial for providing a thorough description of the system.

For these reasons, it is expected that advanced NMR techniques will be used increasingly in the near future in the consolidated, but still fruitful and rapidly evolving, field of halogen bonding in solution.

Conflicts of Interest: The author declares no conflict of interest.

References and Notes

- Hassel, O.; Hvoslef, J. The Structure of Bromine 1,4-Dioxanate. *Acta Chem. Scand.* **1954**, *8*, 873. [[CrossRef](#)]
- Hassel, O. Structural aspects of interatomic charge-transfer bonding. *Science* **1970**, *170*, 497–502. [[CrossRef](#)] [[PubMed](#)]
- Cavallo, G.; Metrangolo, P.; Milani, R.; Pilati, T.; Priimagi, A.; Resnati, G.; Terraneo, G. The Halogen Bond. *Chem. Rev.* **2016**, *116*, 2478–2601. [[CrossRef](#)] [[PubMed](#)]
- Beale, T.M.; Chudzinski, M.G.; Sarwar, M.G.; Taylor, M.S. Halogen bonding in solution: Thermodynamics and applications. *Chem. Soc. Rev.* **2013**, *42*, 1667–1680. [[CrossRef](#)] [[PubMed](#)]
- Bulfield, D.; Huber, S.M. Halogen Bonding in Organic Synthesis and Organocatalysis. *Chem. Eur. J.* **2016**, *22*, 14434–14450. [[CrossRef](#)] [[PubMed](#)]
- Kolár, M.H.; Hobza, P. Computer Modeling of Halogen Bonds and Other σ -Hole Interactions. *Chem. Rev.* **2016**, *116*, 5155–5187. [[CrossRef](#)] [[PubMed](#)]
- Wang, H.; Wang, W.; Jin, W.J. σ -Hole Bond vs π -Hole Bond: A Comparison Based on Halogen Bond. *Chem. Rev.* **2016**, *116*, 5072–5104. [[CrossRef](#)] [[PubMed](#)]

8. Desiraju, G.R.; Ho, P.S.; Kloo, L.; Legon, A.C.; Marquardt, R.; Metrangolo, P.; Politzer, P.; Resnati, G.; Rissanen, K. Definition of the Halogen Bond (IUPAC Recommendations 2013). *Pure Appl. Chem.* **2013**, *85*, 1711–1713. [[CrossRef](#)]
9. Zhang, Q.; Xu, Z.; Shi, J.; Zhu, W. The Underestimated Halogen Bonds Forming with Protein Backbone in Protein Data Bank. *J. Chem. Inf. Model.* **2017**, *57*, 1529–1534. [[CrossRef](#)] [[PubMed](#)]
10. Aragoni, M.C.; Arca, M.; Devillanova, F.A.; Isaia, F.; Lippolis, V. Adducts of S/Se Donors with Dihalogens as a Source of Information for Categorizing the Halogen Bonding. *Cryst. Growth Des.* **2012**, *12*, 2769–2779. [[CrossRef](#)]
11. Poznański, J.; Poznańska, A.; Shugar, D. A Protein Data Bank Survey Reveals Shortening of Intermolecular Hydrogen Bonds in Ligand-Protein Complexes When a Halogenated Ligand Is an H-Bond Donor. *PLoS ONE* **2014**, *6*, e99984. [[CrossRef](#)] [[PubMed](#)]
12. Mooibroek, T.J.; Gamez, P. Halogen bonding versus hydrogen bonding: What does the Cambridge Database reveal? *Cryst. Eng. Comm.* **2013**, *15*, 4565–4570. [[CrossRef](#)]
13. Wang, Y.; Wu, W.; Liu, Y.; Lu, Y. Influence of transition metal coordination on halogen bonding: CSD survey and theoretical study. *Chem. Phys. Lett.* **2013**, *578*, 38–42. [[CrossRef](#)]
14. Farina, A.; Meille, S.V.; Messina, M.T.; Metrangolo, P.; Resnati, G.; Vecchio, G. Resolution of Racemic 1,2-Dibromohexa-fluoropropane through Halogen-Bonded Supramolecular Helices. *Angew. Chem. Int. Ed. Engl.* **1999**, *38*, 2433–2436. [[CrossRef](#)]
15. Takeuchi, T.; Minato, Y.; Takase, M.; Shinmori, H. Molecularly Imprinted Polymers with Halogen Bonding-Based Molecular Recognition Sites. *Tetrahedron Lett.* **2005**, *46*, 9025–9027. [[CrossRef](#)]
16. Martí-Rujas, J.; Meazza, L.; Keat Lim, G.; Terraneo, G.; Pilati, T.; Harris, K.D.M.; Metrangolo, P.; Resnati, G. An Adaptable and Dynamically Porous Organic Salt Traps Unique Tetrahalide Dianions. *Angew. Chem. Int. Ed.* **2013**, *52*, 13444–13448. [[CrossRef](#)] [[PubMed](#)]
17. Nguyen, H.L.; Horton, P.N.; Hursthouse, M.B.; Legon, A.C.; Bruce, D.W. Halogen Bonding: A New Interaction for Liquid Crystal Formation. *J. Am. Chem. Soc.* **2004**, *126*, 16–17. [[CrossRef](#)] [[PubMed](#)]
18. Bolton, O.; Lee, K.; Kim, H.-J.; Lin, K.Y.; Kim, J. Activating Efficient Phosphorescence from Purely Organic Materials by Crystal Design. *Nat. Chem.* **2011**, *3*, 205–210. [[CrossRef](#)] [[PubMed](#)]
19. Yan, D.; Delori, A.; Lloyd, G.O.; Friščić, T.; Day, G.M.; Jones, W.; Lu, J.; Wei, M.; Evans, D.G.; Duan, X. A Cocrystal Strategy to Tune the Luminescent Properties of Stilbene-Type Organic Solid-State Materials. *Angew. Chem. Int. Ed.* **2011**, *50*, 12483–12486. [[CrossRef](#)] [[PubMed](#)]
20. Atzori, M.; Serpe, A.; Deplano, P.; Schlueter, J.A.; Laura Mercuri, M. Tailoring Magnetic Properties of Molecular Materials through Non-Covalent Interactions. *Inorg. Chem. Front.* **2015**, *2*, 108–115. [[CrossRef](#)]
21. Fourmigué, M.; Batail, P. Activation of Hydrogen- and Halogen-Bonding Interactions in Tetrathiafulvalene-Based Crystalline Molecular Conductors. *Chem. Rev.* **2004**, *104*, 5379–5418. [[CrossRef](#)] [[PubMed](#)]
22. Sarwar, M.G.; Dragisić, B.; Dimitrijević, E.; Taylor, M.S. Halogen Bonding between Anions and Iodoperfluoroorganics: Solution-Phase Thermodynamics and Multidentate-Receptor Design. *Chem. Eur. J.* **2013**, *19*, 2050–2058. [[CrossRef](#)] [[PubMed](#)]
23. Sarwar, M.G.; Dragisić, B.; Sagoo, S.; Taylor, M.S. A Tridentate Halogen-Bonding Receptor for Tight Binding of Halide Anions. *Angew. Chem. Int. Ed.* **2010**, *49*, 1674–1677. [[CrossRef](#)] [[PubMed](#)]
24. Gilday, L.C.; White, N.G.; Beer, P.D. Halogen- and hydrogen-bonding triazole-functionalised porphyrin-based receptors for anion recognition. *Dalton Trans.* **2013**, *42*, 15766–15773. [[CrossRef](#)] [[PubMed](#)]
25. Walter, S.M.; Kniep, F.; Herdtweck, E.; Huber, S.M. Halogen-Bond-Induced Activation of a Carbon-Heteroatom Bond. *Angew. Chem. Int. Ed.* **2011**, *50*, 7187–7191. [[CrossRef](#)] [[PubMed](#)]
26. Coulembier, O.; Meyer, F.; Dubois, P. Controlled Room Temperature ROP of L-Lactide by ICl₃: A Simple Halogen-Bonding Catalyst. *Polym. Chem.* **2010**, *1*, 434–437. [[CrossRef](#)]
27. He, W.; Ge, Y.C.; Tan, C.H. Halogen-Bonding-Induced Hydrogen Transfer to C=N Bond with Hantzsch Ester. *Org. Lett.* **2014**, *16*, 3244–3247. [[CrossRef](#)] [[PubMed](#)]
28. Thordarson, P. Determining association constants from titration experiments in supramolecular chemistry. *Chem. Soc. Rev.* **2011**, *40*, 1305–1323. [[CrossRef](#)] [[PubMed](#)]
29. Laurence, C.; Queignec-Cabanetos, M.; Dziembowska, T.; Queignec, R.; Wojtkowiak, B. 1-Iodoacetylenes. 1. Spectroscopic evidence of their complexes with Lewis bases. A spectroscopic scale of soft basicity. *J. Am. Chem. Soc.* **1981**, *103*, 2567–2573. [[CrossRef](#)]

30. Walker, O.J. Absorption spectra of iodine solutions and the influence of the solvent. *Trans. Faraday Soc.* **1935**, *31*, 1432–1438. [[CrossRef](#)]
31. Erdélyi, M. Halogen bonding in solution. *Chem. Soc. Rev.* **2012**, *41*, 3547–3557. [[CrossRef](#)] [[PubMed](#)]
32. Webb, J.E.A.; Crossley, M.J.; Turner, P.; Thordarson, P. Pyromellitimide Aggregates and Their Response to Anion Stimuli. *J. Am. Chem. Soc.* **2007**, *129*, 7155–7162. [[CrossRef](#)] [[PubMed](#)]
33. Pastor, A.; Martínez-Viviente, E. NMR spectroscopy in coordination supramolecular chemistry: A unique and powerful methodology. *Coord. Chem. Rev.* **2008**, *252*, 2314–2345. [[CrossRef](#)]
34. Ciancaleoni, G.; Zuccaccia, C.; Zuccaccia, D.; Macchioni, A. *Techniques in Inorganic Chemistry*; Fackler, J.P., Jr., Falvello, L., Eds.; CRC: Boca Raton, FL, USA, 2011; pp. 129–180, ISBN 978-1-4398-1514-4.
35. Macchioni, A.; Ciancaleoni, G.; Zuccaccia, C.; Zuccaccia, D. Diffusion Ordered NMR Spectroscopy (DOSY). In *Supramolecular Chemistry: From Molecules to Nanomaterial*; Gale, P.A., Steed, J.W., Eds.; John Wiley & Sons, Ltd.: New York, NY, USA, 2012; Volume 2, Chapter 4; ISBN 978-0-470-74640-0.
36. Bellachioma, G.; Ciancaleoni, G.; Zuccaccia, C.; Zuccaccia, D.; Macchioni, A. NMR investigation of non-covalent aggregation of coordination compounds ranging from dimers and ion pairs up to nano-aggregates. *Coord. Chem. Rev.* **2008**, *252*, 2224–2238. [[CrossRef](#)]
37. Rocchigiani, L.; Macchioni, A. Disclosing the multi-faceted world of weakly interacting inorganic systems by means of NMR spectroscopy. *Dalton Trans.* **2016**, *45*, 2785–2790. [[CrossRef](#)] [[PubMed](#)]
38. Neuhaus, D.; Williamson, M. *The Nuclear Overhauser Effect in Structural and Conformational Analysis*, 2nd ed.; WILEY-VCH: New York, NY, USA, 2000; ISBN 978-0-471-24675-6.
39. Stilbs, P. Fourier transform pulsed-gradient spin-echo studies of molecular diffusion. *Prog. Nucl. Magn. Reson. Spectrosc.* **1987**, *19*, 1–45. [[CrossRef](#)]
40. Price, W.S. Pulsed-field gradient nuclear magnetic resonance as a tool for studying translational diffusion. Part I. Basic theory. *Concepts Magn. Res.* **1997**, *9*, 299–336. [[CrossRef](#)]
41. Price, W.S. Pulsed-field gradient nuclear magnetic resonance as a tool for studying translational diffusion. Part II. Experimental aspects. *Concepts Magn. Res.* **1998**, *10*, 197–237. [[CrossRef](#)]
42. Bertrán, J.F.; Rodríguez, M. Detection of halogen bond formation by correlation of proton solvent shifts. 1. Haloforms in n-electron donor solvents. *Org. Magn. Reson.* **1979**, *12*, 92–94. [[CrossRef](#)]
43. Metrangolo, P.; Resnati, G. Halogen Bonding: A Paradigm in Supramolecular Chemistry. *Chem. Eur. J.* **2001**, *7*, 2511–2519. [[CrossRef](#)]
44. Carlsson, A.-C.C.; Veiga, A.X.; Erdelyi, M. Halogen Bonding in Solution. *Top. Curr. Chem.* **2015**, *359*, 49–76. [[CrossRef](#)] [[PubMed](#)]
45. Thorson, R.A.; Woller, G.R.; Driscoll, Z.L.; Geiger, B.E.; Moss, C.A.; Schlapper, A.L.; Speetzen, E.D.; Bosch, E.; Erdélyi, M.; Bowling, N.P. Intramolecular Halogen Bonding in Solution: ¹⁵N, ¹³C, and ¹⁹F NMR Studies of Temperature and Solvent Effects. *Eur. J. Org. Chem.* **2015**, *2015*, 1685–1695. [[CrossRef](#)]
46. Hakkert, S.B.; Gräfenstein, J.; Erdelyi, M. The ¹⁵N NMR chemical shift in the characterization of weak halogen bonding in solution. *Faraday Discuss.* **2017**. [[CrossRef](#)] [[PubMed](#)]
47. Maugeri, L.; Asencio-Hernández, J.; Lébl, T.; Cordes, D.B.; Slawin, A.M.Z.; Delsuc, M.-A.; Philp, D. Neutral iodotriazoles as scaffolds for stable halogen-bonded assemblies in solution. *Chem. Sci.* **2016**, *7*, 6422–6428. [[CrossRef](#)] [[PubMed](#)]
48. Webb, J.A.; Klijn, J.E.; Hill, P.A.; Bennett, J.L.; Goroff, N.S. Experimental Studies of the ¹³C NMR of Iodoalkynes in Lewis-Basic Solvents. *J. Org. Chem.* **2004**, *69*, 660–664. [[CrossRef](#)] [[PubMed](#)]
49. Ma, N.; Zhang, Y.; Ji, B.; Tian, A.; Wang, W. Structural Competition between Halogen Bonds and Lone-Pair... π Interactions in Solution. *Chem. Phys. Chem.* **2012**, *13*, 1411–1414. [[CrossRef](#)] [[PubMed](#)]
50. Rocchigiani, L.; Ciancaleoni, G.; Zuccaccia, C.; Macchioni, A. Probing the Association of Frustrated Phosphine—Borane Lewis Pairs in Solution by NMR Spectroscopy. *J. Am. Chem. Soc.* **2014**, *136*, 112–115. [[CrossRef](#)] [[PubMed](#)]
51. Korenaga, T.; Shoji, T.; Onoue, K.; Sakai, T. Demonstration of the existence of intermolecular lone pair... π interaction between alcoholic oxygen and the C₆F₅ group in organic solvent. *Chem. Commun.* **2009**, 4678–4680. [[CrossRef](#)] [[PubMed](#)]
52. Viger-Gravel, J.; Leclerc, S.; Korobkov, I.; Bryce, D.L. Correlation between ¹³C chemical shifts and the halogen bonding environment in a series of solid para-diiodotetrafluorobenzene complexes. *CrystEngComm* **2013**, *15*, 3168–3177. [[CrossRef](#)]

53. Vioglio, P.C.; Chierotti, M.R.; Gobetto, R. Solid-state nuclear magnetic resonance as a tool for investigating the halogen bond. *Cryst. Eng. Comm.* **2016**, *18*, 9173–9184. [CrossRef]
54. Vioglio, P.C.; Catalano, L.; Vasylyeva, V.; Nervi, C.; Chierotti, M.R.; Resnati, G.; Gobetto, R.; Metrangolo, P. Natural Abundance ¹⁵N and ¹³C Solid-State NMR Chemical Shifts: High Sensitivity Probes of the Halogen Bond Geometry. *Chem. Eur. J.* **2016**, *22*, 16819–16828. [CrossRef] [PubMed]
55. Cabot, R.; Hunter, C.A. Non-covalent interactions between iodo-perfluorocarbons and hydrogen bond acceptors. *Chem. Commun.* **2009**, 2005–2007. [CrossRef] [PubMed]
56. Shen, Q.J.; Jin, W.J. Strong halogen bonding of 1,2-diiodoperfluoroethane and 1,6-diiodoperfluorohexane with halide anions revealed by UV-Vis, FT-IR, NMR spectroscopies and crystallography. *Phys. Chem. Chem. Phys.* **2011**, *13*, 13721–13729. [CrossRef] [PubMed]
57. Liu, Z.-X.; Sun, Y.; Feng, Y.; Chen, H.; He, Y.-M.; Fan, Q.-H. Halogen-Bonding for Visual Chloride Ion Sensing: A Case Study Using Supramolecular Poly(aryl ether) Dendritic Organogel System. *Chem. Commun.* **2016**, *52*, 2269–2272. [CrossRef] [PubMed]
58. Mungalpara, D.; Stegmüller, S.; Kubik, S. A neutral halogen bonding macrocyclic anion receptor based on a pseudocyclopentapeptide with three 5-iodo-1,2,3-triazole subunits. *Chem. Commun.* **2017**, *53*, 5095–5098. [CrossRef] [PubMed]
59. Noggle, J.H.; Schirmer, R.E. *The Nuclear Overhauser Effect*; Academic Press: New York, NY, USA, 1971; ISBN 9780323141390.
60. Keeler, J. *Understanding NMR Spectroscopy*. 2002. Available online: <http://www.keeler.ch.cam.ac.uk/lectures/Irvine/> (accessed on 28 August 2017).
61. Ciancaleoni, G.; Bertani, R.; Rocchigiani, L.; Sgarbossa, P.; Zuccaccia, C.; Macchioni, A. Discriminating Halogen-Bonding from Other Noncovalent Interactions by a Combined NOE NMR/DFT Approach. *Chem. Eur. J.* **2015**, *21*, 440–447. [CrossRef] [PubMed]
62. Zuccaccia, C.; Bellachioma, G.; Cardaci, G.; Macchioni, A. Solution structure investigation of Ru(II) complex ion pairs: Quantitative NOE measurements and determination of average interionic distances. *J. Am. Chem. Soc.* **2001**, *123*, 11020–11028. [CrossRef] [PubMed]
63. Zuccaccia, C.; Bellachioma, G.; Cardaci, G.; Macchioni, A. Specificity of interionic contacts and estimation of average interionic distances by NOE NMR measurements in solution of cationic Ru(II) organometallic complexes bearing unsymmetrical counterions. *Organometallics* **1999**, *18*, 1–3. [CrossRef]
64. Ciancaleoni, G.; Zuccaccia, C.; Zuccaccia, D.; Macchioni, A. Diffusion and NOE NMR studies on the interactions of neutral amino-acidate arene ruthenium(II) supramolecular aggregates with ions and ion pairs. *Magn. Reson. Chem.* **2008**, *46*, S72–S79. [CrossRef] [PubMed]
65. Geldbach, T. J.; Ruegger, H.; Pregosin, P. S. NOESY, HOESY, T1 and solid-state NMR studies on [RuH(h6-toluene)(Binap)](CF₃SO₃): A molecule with a strongly distorted piano-stool structure. *Magn. Reson. Chem.* **2003**, *41*, 703–708. [CrossRef]
66. Lingscheid, Y.; Arenz, S.; Giernoth, R. Heteronuclear NOE Spectroscopy of Ionic Liquids. *Chem. Phys. Chem.* **2012**, *13*, 261–266. [CrossRef] [PubMed]
67. Braun, D.; Steinhauser, O. The intermolecular NOE is strongly influenced by dynamics. *Phys. Chem. Chem. Phys.* **2015**, *17*, 8509–8517. [CrossRef] [PubMed]
68. Gabl, S.; Schröder, C.; Braun, D.; Weingärtner, H.; Steinhauser, O. Pair dynamics and the intermolecular nuclear Overhauser effect (NOE) in liquids analysed by simulation and model theories: Application to an ionic liquid. *J. Chem. Phys.* **2012**, *140*, 184503. [CrossRef] [PubMed]
69. Crank, J. *The Mathematics of Diffusion*, 2nd ed.; Clarendon Press: Oxford, UK, 1975; ISBN 978-0198534112.
70. Einstein, A. *Investigations in the Theory of Brownian Movements*; Dover: New York, NY, USA, 1956; ISBN 9781607962854.
71. Hahn, E.L. Spin echoes. *Phys. Rev.* **1950**, *80*, 580–594. [CrossRef]
72. Stejskal, E.O.; Tanner, J.E. Spin diffusion measurements: Spin echoes in the presence of a time-dependent field gradient. *J. Chem. Phys.* **1965**, *42*, 288–292. [CrossRef]
73. Macchioni, A.; Ciancaleoni, G.; Zuccaccia, C.; Zuccaccia, D. Determining accurate molecular sizes in solution through NMR diffusion spectroscopy. *Chem. Soc. Rev.* **2008**, *37*, 479–489. [CrossRef] [PubMed]
74. By using this formulation, the effect of T_2 can be neglected, since it is the same with and without G .
75. Edward, J.T. Molecular volumes and the Stokes-Einstein equation. *J. Chem. Educ.* **1970**, *47*, 261–270. [CrossRef]

76. Chen, H.-C.; Chen, S.-H. Diffusion of crown ethers in alcohols. *J. Phys. Chem.* **1984**, *88*, 5118–5121. [[CrossRef](#)]
77. Sinnaeve, D. Simultaneous solvent and J-modulation suppression in PGSTE-based diffusion experiments. *J. Magn. Res.* **2014**, *245*, 24–30. [[CrossRef](#)] [[PubMed](#)]
78. Chen, A.; Wu, D.; Johnson, C.S., Jr. Determination of Molecular Weight Distributions for Polymers by Diffusion-Ordered NMR. *J. Am. Chem. Soc.* **1995**, *117*, 7965–7970. [[CrossRef](#)]
79. Marega, R.; Aroulmoji, V.; Bergamin, M.; Feruglio, L.; Dinon, F.; Bianco, A.; Murano, E.; Prato, M. Two-Dimensional Diffusion-Ordered NMR Spectroscopy as a Tool for Monitoring Functionalized Carbon Nanotube Purification and Composition. *ACS Nano* **2010**, *4*, 2051–2058. [[CrossRef](#)] [[PubMed](#)]
80. Rocchigiani, L.; Bellachioma, G.; Ciancaleoni, G.; Crocchianti, S.; Lagana, A.; Zuccaccia, C.; Zuccaccia, D.; Macchioni, A. Anion-Dependent Tendency of Di-Long-Chain Quaternary Ammonium Salts to Form Ion Quadruples and Higher Aggregates in Benzene. *Chem. Phys. Chem.* **2010**, *11*, 3243–3254. [[CrossRef](#)] [[PubMed](#)]
81. Pettirossi, S.; Bellachioma, G.; Ciancaleoni, G.; Zuccaccia, C.; Zuccaccia, D.; Macchioni, A. Diffusion and NOE NMR Studies on Multicationic DAB-Organoruthenium Dendrimers: Size-Dependent Noncovalent Self-Assembly to Megamers and Ion Pairing. *Chem. Eur. J.* **2009**, *15*, 5337–5347. [[CrossRef](#)] [[PubMed](#)]
82. Pregosin, P.S. NMR diffusion methods in inorganic and organometallic chemistry. *Spectrosc. Prop. Inorg. Organomet. Compd.* **2011**, *42*, 248–268. [[CrossRef](#)]
83. Rocchigiani, L.; Busico, V.; Pastore, A.; Macchioni, A. Probing the interactions between all components of the catalytic pool for homogeneous olefin polymerisation by diffusion NMR spectroscopy. *Dalton Trans.* **2013**, *42*, 9104–9111. [[CrossRef](#)] [[PubMed](#)]
84. Allouche, L.; Marquis, A.; Lehn, J.M. Discrimination of Metallosupramolecular Architectures in Solution by Using Diffusion Ordered Spectroscopy (DOSY) Experiments: Double-Stranded Helicates of Different Lengths. *Chem. Eur. J.* **2006**, *12*, 7520–7525. [[CrossRef](#)] [[PubMed](#)]
85. Ciancaleoni, G.; Zuccaccia, C.; Zuccaccia, D.; Clot, E.; Macchioni, A. Self-Aggregation Tendency of All Species Involved in the Catalytic Cycle of Bifunctional Transfer Hydrogenation. *Organometallics* **2009**, *28*, 960–967. [[CrossRef](#)]
86. Tatko, C.D.; Waters, M.L. Effect of Halogenation on Edge—Face Aromatic Interactions in a β -Hairpin Peptide: Enhanced Affinity with Iodo-Substituents. *Org. Lett.* **2006**, *6*, 3969–3972. [[CrossRef](#)] [[PubMed](#)]
87. Serpell, C.J.; Kila, N.L.; Costa, P.J.; Félix, V.; Beer, P.D. Halogen Bond Templated Assembly of an Imidazolium Pseudorotaxane. *Angew. Chem. Int. Ed.* **2010**, *49*, 5322–5326. [[CrossRef](#)] [[PubMed](#)]
88. Gilday, L.C.; Beer, P.D. Halogen- and Hydrogen-Bonding catenanes for Halide-Anion Recognition. *Chem. Eur. J.* **2014**, *20*, 8379–8385. [[CrossRef](#)] [[PubMed](#)]
89. Huber, S.M.; Scanlon, J.D.; Jimenez-Izal, E.; Ugalde, J.M.; Infante, I. On the directionality of halogen bonding. *Phys. Chem. Chem. Phys.* **2013**, *15*, 10350–10357. [[CrossRef](#)] [[PubMed](#)]
90. Politzer, P.; Murray, J.S.; Clark, T. Halogen Bonding: An Electrostatically-Driven Highly Directional Noncovalent Interaction. *Phys. Chem. Chem. Phys.* **2010**, *12*, 7748–7757. [[CrossRef](#)] [[PubMed](#)]
91. Kozuch, S.; Martin, J.M.L. Halogen Bonds: Benchmarks and Theoretical Analysis. *J. Chem. Theory Comput.* **2013**, *9*, 1918–1931. [[CrossRef](#)] [[PubMed](#)]
92. Yan, X.Q.; Zhao, X.R.; Wang, H.; Jin, W.J. The Competition of σ -Hole...Cl⁻ and π -Hole...Cl⁻ Bonds between C₆F₅X (X = F, Cl, Br, I) and the Chloride Anion and Its Potential Application in Separation Science. *J. Phys. Chem. B* **2014**, *118*, 1080–1087. [[CrossRef](#)] [[PubMed](#)]
93. Cao, J.; Yan, X.; He, W.; Li, X.; Li, Z.; Mo, Y.; Liu, M.; Jiang, Y.-B. C–I... π Halogen Bonding Driven Supramolecular Helix of Bilateral N-Amidothiouras Bearing β -Turns. *J. Am. Chem. Soc.* **2017**, *139*, 6605–6610. [[CrossRef](#)] [[PubMed](#)]
94. In the author's opinion, NOESY and peak intensities should have been coupled with a simple DOSY experiment (see below) that would have proved the existence of supramolecular oligomers more effectively.
95. Casnati, A.; Liantonio, R.; Metrangolo, P.; Resnati, G.; Ungaro, R.; Ugozzoli, F. Molecular and Supramolecular Homochirality: Enantiopure Perfluorocarbon Rotamers and Halogen-Bonded Fluorous Double Helices. *Angew. Chem. Int. Ed.* **2006**, *45*, 1915–1918. [[CrossRef](#)] [[PubMed](#)]
96. Danelius, E.; Andersson, H.; Jarvoll, P.; Lood, K.; Gräfenstein, J.; Erdélyi, M. Halogen Bonding: A Powerful Tool for Modulation of Peptide Conformation. *Biochemistry* **2017**, *56*, 3265–3272. [[CrossRef](#)] [[PubMed](#)]
97. Carlsson, A.-C.C.; Gräfenstein, J.; Budnjo, A.; Laurila, J.L.; Bergquist, J.; Karim, A.; Kleinmaier, R.; Brath, U.; Erdélyi, M. Symmetric Halogen Bonding Is Preferred in Solution. *J. Am. Chem. Soc.* **2012**, *134*, 5706–5715. [[CrossRef](#)] [[PubMed](#)]

98. Perrin, C.L. Are Short, Low-Barrier Hydrogen Bonds Unusually Strong? *Acc. Chem. Res.* **2010**, *43*, 1550–1557. [[CrossRef](#)] [[PubMed](#)]
99. Macchioni, A. Ion Pairing in Transition-Metal Organometallic Chemistry. *Chem. Rev.* **2005**, *105*, 2039–2074. [[CrossRef](#)] [[PubMed](#)]
100. For example, in $[L^1AuL^2]X$ ion pairs, the positive charge is formally located on the gold, but the anion position depends on the nature of the ligands. See references 101–103.
101. Zuccaccia, D.; Belpassi, L.; Tarantelli, F.; Macchioni, A. Ion Pairing in Cationic Olefin–Gold(I) Complexes. *J. Am. Chem. Soc.* **2009**, *131*, 3170–3171. [[CrossRef](#)] [[PubMed](#)]
102. Ciancaleoni, G.; Belpassi, L.; Tarantelli, F.; Zuccaccia, D.; Macchioni, A. A combined NMR/DFT study on the ion pair structure of $[(PR^1_2R^2)Au(\eta^{2-3}\text{-hexyne})]BF_4$ complexes. *Dalton Trans.* **2013**, *42*, 4122–4131. [[CrossRef](#)] [[PubMed](#)]
103. Biasiolo, L.; Ciancaleoni, G.; Belpassi, L.; Bistoni, G.; Macchioni, A.; Tarantelli, F.; Zuccaccia, D. Relationship between the anion/cation relative orientation and the catalytic activity of nitrogen acyclic carbene–gold catalysts. *Catal. Sci. Technol.* **2015**, *5*, 1558–1567. [[CrossRef](#)]
104. Bedin, M.; Karim, A.; Reitti, M.; Carlsson, A.-C.C.; Topić, F.; Cetina, M.; Pan, F.; Havel, V.; Al-Ameri, F.; Sindelar, V.; et al. Counterion influence on the N–I–N halogen bond. *Chem. Sci.* **2015**, *6*, 3746–3756. [[CrossRef](#)]
105. Karim, A.; Reitti, M.; Carlsson, A.-C.C.; Gräfenstein, J.; Erdélyi, M. The nature of $[N-Cl-N]^+$ and $[N-F-N]^+$ halogen bonds in solution. *Chem. Sci.* **2014**, *5*, 3226–3233. [[CrossRef](#)]
106. Zapata, F.; Caballero, A.; White, N.G.; Claridge, T.D.W.; Costa, P.J.; Félix, V.; Beer, P.D. Fluorescent Charge-Assisted Halogen-Bonding Macrocyclic Halo-Imidazolium Receptors for Anion Recognition and Sensing in Aqueous Media. *J. Am. Chem. Soc.* **2012**, *134*, 11533–11541. [[CrossRef](#)] [[PubMed](#)]
107. Ciancaleoni, G.; Macchioni, A.; Rocchigiani, L.; Zuccaccia, C. A PGSE NMR approach to the characterization of single and multi-site halogen-bonded adducts in solution. *RSC Adv.* **2016**, *6*, 80604–80612. [[CrossRef](#)]
108. If inter-penetrating adducts are involved, as in the case of helices or cages, this could be not true.
109. If the adduct and the components are not in rapid exchange, the Equation (11) is not valid anymore. But the kinetics of XB formation is generally very fast.
110. Belpassi, L.; Infante, I.; Tarantelli, F.; Visscher, L. The Chemical Bond between Au(I) and the Noble Gases. Comparative Study of $NgAuF$ and $NgAu^+$ ($Ng = Ar, Kr, Xe$) by Density Functional and Coupled Cluster Methods. *J. Am. Chem. Soc.* **2008**, *130*, 1048–1060. [[CrossRef](#)] [[PubMed](#)]
111. Ciancaleoni, G.; Santi, C.; Ragni, M.; Braga, A.M. Charge-displacement analysis as a tool to study chalcogen bonded adducts and predict their association constants in solution. *Dalton Trans.* **2015**, *44*, 20168–20175. [[CrossRef](#)] [[PubMed](#)]
112. Ciancaleoni, G.; Belpassi, L.; Marchetti, F. Back-Donation in High-Valent d^0 Metal Complexes: Does It Exist? The Case of Nb^V . *Inorg. Chem.* **2017**, *56*, 11266–11274. [[CrossRef](#)] [[PubMed](#)]
113. Bistoni, G.; Rampino, S.; Scafuri, N.; Ciancaleoni, G.; Zuccaccia, D.; Belpassi, L.; Tarantelli, F. How π back-donation quantitatively controls the CO stretching response in classical and non-classical metal carbonyl complexes. *Chem. Sci.* **2016**, *7*, 1174–1184. [[CrossRef](#)]
114. Raatikainen, K.; Rissanen, K. Interaction between amines and N-haloimides: A new motif for unprecedentedly short $Br \cdots N$ and $I \cdots N$ halogen bonds. *CrystEngComm* **2011**, *13*, 6972–6977. [[CrossRef](#)]

